Size-asymmetrical Lennard-Jones solid solutions: Interstitials and substitutions

This manuscript was accepted by J. Chem. Phys. Click here to see the version of record.

Ziwei Guo (郭子威) and James T. Kindt[a)]

Department of Chemistry, Emory University, Atlanta, Georgia, USA, 30322

Abstract

We present simulation studies of solid solutions formed upon compression of mixtures of Lennard-Jones (LJ) particles with diameter ratios 2:1 and 3:1. Grand canonical Monte Carlo (GCMC) and Gibbs-Duhem integration were used to determine the compositions of coexisting solid and liquid phases at several pressures and fixed temperature. Concentrations of small particles dissolved in interstitial sites of the large-particle lattice, under liquid-solid coexistence conditions, were determined directly from GCMC simulations. Indirect methods were used to calculate levels of small particles dissolved substitutionally, either singly or in plural, with the average number of small solutes occupying a lattice site vacated by a large particle increasing with higher pressure. In the cases studied, the fraction of small solutes occupying these substitutional sites was found to be small (2% or lower, depending on the mixture and conditions), but to stay roughly constant with increasing pressure. Structural and dynamic characteristics of the solid solutions are described and compared with reported characteristics of the related interstitial solid solution formed by hard spheres.

1. Introduction

Solid solutions or alloys, mixtures in which one component is distributed in a disordered arrangement throughout an otherwise regular crystal structure, have been widely studied due to their applications in photonics, optics, semiconductors and structure design[1-5]. In a substitutional solid solution (SSS), impurity particles occupy some fraction of lattice sites in place of the majority component particles; the prototypical example is bronze, which contains tin substituted within a copper lattice. In an interstitial solid solution (ISS) the impurity component occupies some fraction of the interstitial positions of the crystalline lattice of the first species; the prototypical example is steel, with carbon atoms occupying interstitial sites in an iron lattice[6]. The presence of the impurities may have important effects on the mechanical behaviors, phase diagrams, and electrical properties of the solids, and the ability to tune the

[a)] jkindt@emory.edu

properties by adjusting the amount and nature of the minority components have made solid solutions tremendously important in technology.

One obvious distinction between substitutional and interstitial localization of impurities is that the former is more likely for impurities that are similar in size to the primary component, while the latter is more likely for impurities that are significantly smaller. It is natural to speculate, then, about whether a dimer or cluster of small impurities can play the role of a large impurity and form plural substitutional defects within a primarily interstitial crystal. Colloidal crystals have been predicted and synthesized in which icosahedral clusters of 13 small "B" spheres occupy sites similar (though not identical) to large "A" spheres[7], although this is a compound with a fixed stoichiometry of AB_{13} and not an alloy. Density functional theory (DFT) calculations suggest that vacancy sites within carbon steel will be occupied by a carbon dimer[8]. Vacancy occupation by one or more impurity particles present interstitially and the equilibrium thermodynamics of vacancy levels has been addressed in the recent metallurgical literature[9], and appears to have implications for design of advance materials with many thermodynamic and kinetic properties like High Entropy Alloys (HEAs) with much better resistance to radiation damages.

To gain some general perspective on whether interstitial and plural substitutional impurities might appear in the same phase we have investigated size-asymmetrical binary Lennard-Jones (LJ) solid solutions, with the smaller particle the minority component, at coexistence with the binary liquid mixture. The composition at the coexistence point is of interest as represents the highest impurity content that the solid can absorb at a given pressure and temperature without becoming unstable with respect to phase separation.

Binary mixtures of LJ solids have been studied for decades[10-16]. However, only few studies focus on the ISS phase of LJ solids, which treat the species in interstitial places as impurity[17-18]. There are multiple approaches to study the solid-liquid phase coexistence for LJ systems. Ferreira *et al*. obtained the solid-liquid coexistence by absolute free energy calculations[1]. Gibbs ensemble simulation has been extended to simulate the solid-liquid phase equilibrium by Quirke *et al*[19]. Escobedo *et al*. applied virtual Gibbs ensemble to directly simulate the solid-liquid phase coexistence[20]. A phase-switch Monte Carlo was developed by Errington to investigate the coexistence[21]. Cottin *et al*. studied the phase equilibrium of binary LJ mixtures from a cell theory approach[22]. MD simulation is also used to study the crystal growth in binary LJ mixtures at liquid-solid interfaces[23]. A widely used current method to study the solid-liquid phase equilibrium is Gibbs-Duhem integration developed by Kofke[24-25]. With the prior knowledge of one coexistence point, one can integrate starting from the existing point using

the Clapeyron formula to find the coexistence point at new temperature. Hall *et al*. reported the solid-liquid phase diagram of the binary LJ mixtures in the temperature-composition plane at fixed pressure by Gibbs-Duhem integration with MC simulation[26-27].

Here, we employ a variation of Gibbs-Duhem integration to track the coexistence points at different pressures with fixed temperature. We start from the coexistence point for a pure large species LJ system whose phase coexistence data is available from the literature[1], then used Gibbs-Duhem integration to get the new coexistence point at higher pressure with some small species present using grand canonical Monte Carlo simulation (GCMC). The solid phases would actually describe an ISS phase in which the large species forms a face centered-cubic (fcc) lattice while the small impurity species primarily occupy the interstices, but may also occupy the main lattice positions either singly or in clusters. Three systems were studied in this work. The mixtures in two cases have the same ϵ but different sizes, with σ ratios 1:2 and 1:3. (system S2 and S3 as shown in Table (I)). In the third case (system E2 as shown in Table (I)) the large particles are more strongly attractive than the small component (σ ratio 1:2, ϵ ratio 1:1.5), mirroring the typical trend in experimental systems like neopentane/methane[28]. For all systems, we studied the coexistence points under three pressures (6.0, 8.0 and 10.0 $k_B T/\sigma_{LL}{}^3$) and performed structural analysis on the liquid phase and solid phase. To investigate the substitution behavior by the small components, we created a vacancy in the large-particle lattice manually, and observed the occupation of the vacancy by small particles at the chemical potential determined for the system at coexistence. Using standard approaches to estimate the free energy of vacancy formation[29-30], we then used the occupation statistics to estimate the concentration of all vacancies (substituted or empty) for each system.

2. Methods

2.1 Determination of solid-liquid coexistence points

The Gibbs-Duhem integration method is commonly applied to track how the pressure at coexistence between two phases varies with temperature[25], and has also been applied to find the variation of coexisting compositions with changing T (at fixed pressure) in a binary mixture[27]. Here we consider the application of the same strategy while fixing T and varying pressure.

The solid-liquid phase coexistence point of LJ system can be accessed via various methods[1]. With the densities of solid and liquid phases at coexistence at a specified temperature and

pressure P_0 obtained from the literature, Grand Canonical Monte Carlo (GCMC) can be used to determine the chemical potential of the liquid state (and by extension, the solid). Given the Gibbs-Duhem equation:

$$\sum_{i=1}^{I} N_i d\mu_i = -SdT + VdP \quad (1)$$

variations in pressure and composition in a binary mixture at constant T are related by:

$$dP = \rho_S d\mu_S + \rho_L d\mu_L \quad (2)$$

where the subscripts designate small (S) and large (L) particles. If we make the approximation that in the solid phase ρ_L is a constant and small particles partition strongly to the liquid phase $\rho_S(solid) \ll \rho_S(liquid)$, the large component's chemical potential at higher pressure $P > P_0$ can be obtained without further information about the small component's behavior:

$$P - P_0 = \rho_L \Delta\mu_L \quad (3)$$

Substituting the chemical potential as fugacity $f = \exp(\beta\mu)$, with the de Broglie thermal wavelength set to 1, we have:

$$P - P_0 = \rho_L ln\frac{f_L}{f_L^0} \quad (4)$$

Since the approximations that produce Eq. (3) and Eq. (4) are not ultimately satisfied, we rely on these equations for a first approximation only. For each pressure P of interest, the liquid phase is first simulated using GCMC with fixed f_L obtained from Eq. (4) and varying f_S to find the value that produces a pressure P in the mixture (Fig. (1)). In principle, simulation of the solid phase at constant f_S, f_L, and V would produce an equilibrated state whose pressure could be compared with P to test the assumptions made above. However, the rigidity of the lattice structure and the need for the lattice spaces to be commensurate with the periodicity imposed by the simulation box make this unreliable. Instead, the solid phase is simulated by GCMC, either at constant P, N_L, and f_S, or at constant P, f_L and f_S, in which case the kinetic barrier to changing the lattice structure imposes an effective fourth constraint on number of cells in the system. Through the simulations at constant P, f_L and f_S, we saw it is a rare event for solid phase having a vacancy, therefore, for efficiency concern, we manually create a vacancy in crystal structure (remove a large particle in simulation box) and run simulations at constant P, N_L, and f_S to find the small species partition in solid phase (Table. (Ⅰ)). The manually created vacancy is implemented in all the following results except the discussions on phase diagrams, small species absorption and radial distribution function (RDF). In any case, we cannot rely on particle exchange moves to ensure that the fugacity of large particles in the solid phase is in fact equal to the f_L of Eq. (4), so we rely again on the Gibbs-Duhem equation.

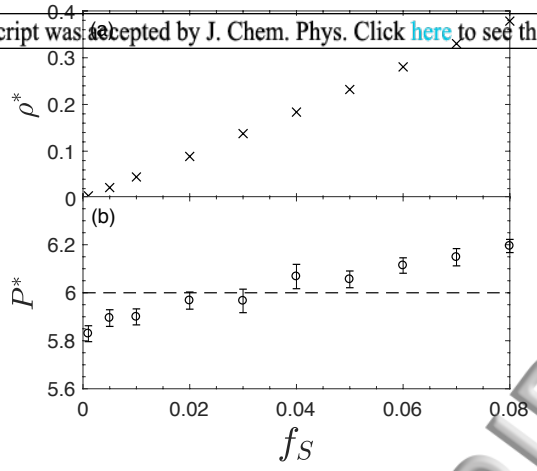

FIG. 1. (a) Number density of small species in system S2 (liquid phase) at different small species fugacity f_S (error bar is smaller than the size of the data points); (b) Pressure of system S2 at different small species fugacity f_S at fixed large species fugacity $f_L = 20.9$, showing method of initial approximation of f_S at coexistence.

At fixed pressure, Gibbs-Duhem equation gives:

$$d\mu_L = -\frac{\rho_S}{\rho_L} d\mu_S \tag{5}$$

Therefore, in order to calculate the $\Delta\mu_L$ to make the correction at μ_L, we need to rewrite $d\mu_S$ first.

We find empirically that ρ_S (in the solid phase, at fixed pressure and N_L) can be related to f_S by the function:

$$\rho_S = \frac{Af_S}{1+Bf_S} = \frac{A\exp(\beta\mu_S)}{1+B\exp(\beta\mu_S)} \tag{6}$$

in which A and B are two constants.

Differentiating Eq. (6):

$$\frac{\partial\rho_S}{\partial\mu_S} = \frac{A\beta\exp(\beta\mu_S)}{[1+B\exp(\beta\mu_S)]^2} \tag{7}$$

So $d\mu_L$ can be rewritten as:

$$d\mu_L = -\frac{\rho_S}{\rho_L} d\mu_S = -\frac{1+B\exp(\beta\mu_S)}{\beta\rho_L} \partial\rho_S \tag{8}$$

From Eq. (6), we have:

$$f_S = \exp(\beta\mu_S) = \frac{\rho_S}{A-B\rho_S} \tag{9}$$

Rewriting Eq. (8) with Eq. (9):

$$d\mu_L = -\frac{1+B\frac{\rho_S}{A-B\rho_S}}{\beta\rho_L}\partial\rho_S \quad (10)$$

Integrating Eq. (10) yields:

$$\Delta\mu_L = \frac{A}{\beta B\rho_L}[\ln\left(1-\frac{B}{A}\rho_S\right)] \quad (11)$$

The new corrected (lower) μ_L calculated from Eq. (11) can then be used in the first step, simulation of the liquid. An increase in the small-particle content of the liquid will then be needed to bring the liquid pressure up to P, and the small-particle fugacity in the solid will also increase. This process is repeated until self-consistency is reached.

2.2 Implementation details

Pairs of particles interact via the Lennard-Jones potential:

$$\Phi_{ij}(r) = 4\epsilon_{ij}[\left(\frac{\sigma_{ij}}{r}\right)^{12} - \left(\frac{\sigma_{ij}}{r}\right)^{6}] \quad (12)$$

The following mixing rule is applied when calculating the cross term of potential energy: $\sigma_{SL} = (\sigma_{SS}+\sigma_{LL})/2$, $\epsilon_{SL} = \sqrt{\epsilon_{SS}\epsilon_{LL}}$. The potential is simply truncated at the cutoff distance $r_{cut} = 4\sigma$. Different r_{cut} are used for three interactions (two interactions among small and large, one cross term of interaction). Periodic boundary conditions with long-range corrections are applied.

In the liquid phase, the equilibration and production periods each consisted of at least 10^6 MC cycles for liquid phase. Each MC cycle contains 50 insertion or removal trials for small species and 150 insertion or removal trials for large species. For solid phase, the equilibration and production periods each consisted of at least 5×10^7 single insertion and removal moves. In both phases, each move was followed by 100 translation moves attempts for small and large species, respectively. The initial solid phase is constructed by 864 LJ particles formed into a fcc lattice. The maximum distance for translation move is set to 0.05 σ_{LL} and 0.01 σ_{LL} for small and large species, respectively. The maximum volume change is set to 0.1 σ_{LL}^3 in constant pressure solid phase simulations. Reduced units, scaled to the large species σ_{LL} and ϵ_{LL}, are used in all the data reported in this work, and all simulations are performed at $k_BT = \epsilon_{LL}$=1. VMD was used for molecular graphics[31].

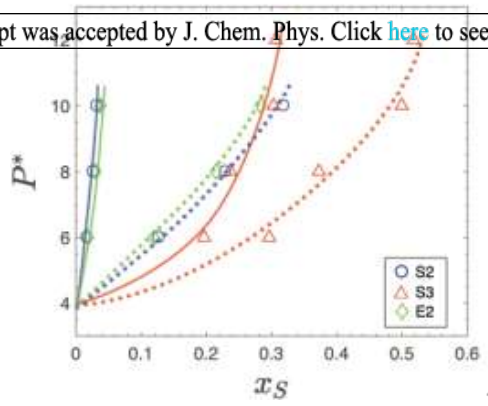

FIG. 2. Solid-liquid phase diagram for three systems at mole fraction (small species)- pressure plane. Curves on the phase boundaries are drawn only as guide to the eye. Solid curves represent the solid boundaries (without the vacancy in solid phase), while dotted lines represent the liquid boundaries. Errors are smaller than the scale of data points.

3. Results and discussion

3.1 Solid-liquid phase coexistence and interstitial absorption

Compositions of liquid and solid solutions of small particles at coexistence (Fig. (2)) have been determined for three systems S2, S3 and E2 (Table (I)) at three pressures using the Gibbs-Duhem integration method described above. The most pronounced difference is that in system S3 (σ ratio 1:3) the solubility of small particles in the solid phase is much greater than in systems S2 or E2 (σ ratio 1:2). The mole fraction of small species in solid phase in system S3 are even comparable to the fractions in liquid phases at coexistence in system S2 and E2. It is interesting to compare this system with the interstitial solid solution of hard spheres (HS) of diameter ratio 0.3:1 studied by Filion and Dijkstra[5]. As in the HS mixture, the small LJ particles primarily occupy octahedral sites in the fcc lattice of the larger particles. Insight into the thermodynamics of absorption into the solid phase can be derived from the variation of fugacity with composition. If the interstitial sites behave as independent single-occupancy sites (as in the Langmuir adsorption isotherm, although this case involves absorption and not adsorption), then the fugacity would increase non-linearly as these sites fill:

$$f = C\,\Theta/(1-\Theta) = C\,x_s/(1-2x_s) \qquad (13)$$

Fig. (3) shows that in the case of system S3, the absorption of small particles within the solid follows a more nearly ideal dependence than predicted from the single-occupancy model. In fact, the radial distribution function (Fig. (4)) for the solid phase mixture of system S3 (and system S2) contains a peak in $g(SS)$ at distances nearer than the nearest small-large neighbor

peak, indicating that impurities do in fact pair up within the interstitial sites. This contrasts with the HS case, where the interstitial solid solution was seen to reach a maximum of number ratio of small to large particles of 1:1. (Higher loading of small particles into the HS solid occurred via a first-order transition to the LS_6 structure where 6 small particles can be found in interstitial sites of a bcc lattice.) The possibility of multiple occupancy in interstitial sites is presumably facilitated by the softer nature of the potential and the attractions between small particles, since reduction in that attraction (system E2) appears to suppress it. We have not accessed high enough pressures to determine whether the interstitial solid solution remains stable up to (or beyond) a mole fraction $x_s = 0.5$ as was seen in the hard-sphere system[5]; an additional data point at P^*=12 generated for system S3 alone yielded x_S of 0.306 in the solid phase at coexistence (Fig. (2)).

The presence of the small particles expands the lattice spacing of the large particles slightly (Table (Ⅱ)). Since the lattice spacing change is very small (<1%), it is still reasonable to approximately estimate the vacancy concentration through the method discussed in next section *3.2*. Higher pressure will suppress the lattice spacing in both pure large systems and mixtures (d in Table (Ⅱ)); the lattice spacing difference between the mixture and pure large system is bigger at higher pressure (Δd in Table (Ⅱ)) due to the presence of more small species in solid solutions.

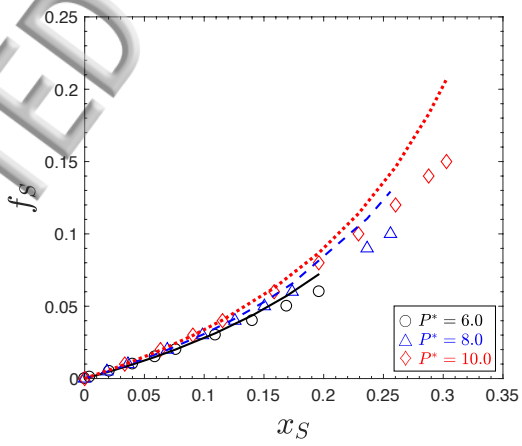

FIG. 3. Fugacity of small species at different mole fraction x_S in system S3 (without the vacancy in solid phase) at different pressures. The fugacity of large species is fixed at 16.99, 99.05 and 527.13, for pressure 6.0, 8.0 and 10.0, respectively. Fitting of data by Langmuir adsorption isotherm are shown in solid, dash, dot lines for pressure 6.0, 8.0 and 10.0, respectively.

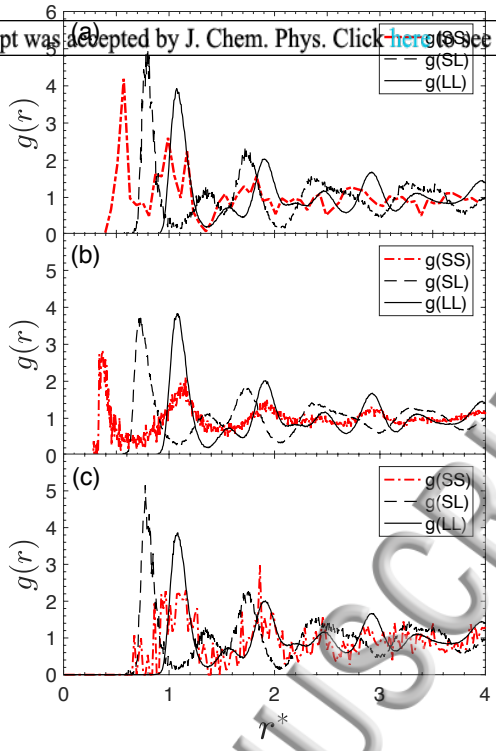

FIG. 4. Radial Distribution Function (RDF) in solid phase without the vacancy for system (a) S2, (b) S3 and (c) E2 at pressure 6.0.

Table Ⅰ. Compositions of solid phases under solid-liquid coexistence conditions for different systems with 863 large particles and 1 vacancy. N_S^{sub} is the average number of small particles per vacancy, N_S^{inter} is the average number of small particles per interstitial site.

system	σ_{LL}: σ_{SS}	ϵ_{LL}: ϵ_{SS}	P^*	ρ_S	N_S^{sub}	N_S^{inter}
	2:1	1:1	6.0	0.018	1.58	0.016
S2	2:1	1:1	8.0	0.029	2.65	0.024
	2:1	1:1	10.0	0.036	3.30	0.029
	3:1	1:1	6.0	0.255	1.30	0.246
S3	3:1	1:1	8.0	0.331	2.53	0.310
	3:1	1:1	10.0	0.479	5.04	0.440
	2:1	1.5:1	6.0	0.019	1.40	0.017
E2	2:1	1.5:1	8.0	0.033	2.30	0.028
	2:1	1.5:1	10.0	0.042	2.89	0.035

Table Ⅱ. Lattice spacing d (defined as the edge length of one fcc unit cell; reduced unit σ_{LL} is used) in different systems; and the expansion Δd observed between the mixtures and pure systems.

P^*	$d_{\text{Pure Large}}$	d_{S2}	Δd_{S2}	d_{S3}	Δd_{S3}	d_{E2}	Δd_{E2}
6.0	1.5618	1.5643	0.0025	1.5717	0.0099	1.5642	0.0024
8.0	1.5467	1.5505	0.0038	1.5572	0.0105	1.5506	0.0039
10.0	1.5346	1.5388	0.0042	1.5492	0.0146	1.5392	0.0046

3.2 Substitutional absorption

Although the small particles appear to favor interstitial sites, we sought to characterize and quantify the substitutional absorption in this system, particularly the possibility of plural substitution, with more than one of the small species occupying a lattice position vacated by a large particle (Fig. (5)). In simulations initiated with a large particle vacancy defect, the average number of dopants occupying the vacancy at coexistence with the mixed liquid is on average greater than one (Table (Ⅰ)). The distribution of occupancy numbers is shown in Fig. (6). We can clearly see the trend that the vacancy tends to have greater occupancy at increasing system pressure. It is somewhat surprising that reducing the dopant diameter from 1/2 to 1/3 of the larger component does not increase the average number of dopants occupying the vacancy at low pressure (although it does increase the occupancy at P^*=10.0). These very small dopants are easily accommodated in the interstitial spaces, where they interact with 6 large particle neighbors without causing steric strain. A single S3 system dopant in the vacancy can only be near to ~3-4 large neighbors simultaneously, and the second or third dopants to occupy a single vacancy are not optimally positioned to interact both with the lattice and with each other (so adsorption to the vacancy is not cooperative). In contrast, the dopants in systems S2 and E2 can fit more easily into the vacancy than into interstitial sites, and successive occupying dopants will be in position to attract each other and the large particles simultaneously.

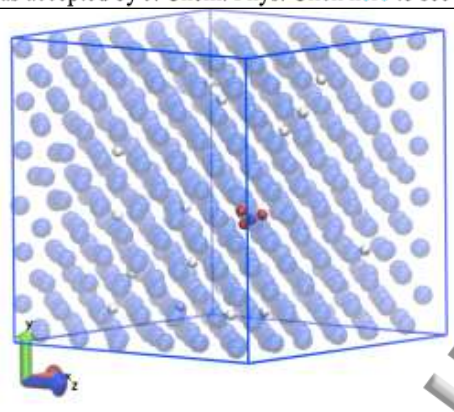

FIG. 5. A snapshot from our simulation for system S2 at pressure 10.0. Large species are shown in transparent blue, small species in interstices are shown in white, and particles in substitution position are shown in red.

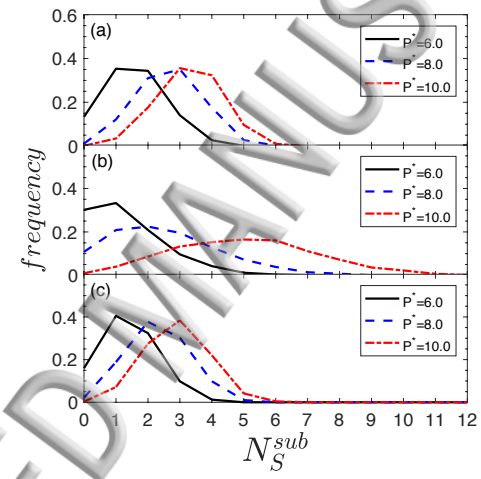

FIG. 6. Distribution of small species substitution in the defect site for system (a) S2, (b) S3 and (c) E2.

We sought then to determine the absolute levels of substitutional absorbates in these systems at coexistence. In principle, we could find vacancy concentrations in the doped solids directly from GCMC, using large particle exchange moves at the fugacities f_L and f_S determined in section *3.1*. We found that conventional single-particle insertion and removal moves were more efficient for this purpose in these systems than the solvent-repacking Monte Carlo algorithm[32-33], but that the overall levels of substitutional defects were too low to obtain good statistics during reasonable simulation times. Instead we used our knowledge of the equilibrium between empty vacancies and singly- or multiply-substituted vacancies under

coexistence conditions, along with estimates of the un-substituted vacancy levels in the pure solid obtained by standard methods[32-33]. Specifically, after defining a spherical subvolume v with a diameter of $1.06\sigma_{LL}$, which is centered at the empty lattice site in a crystal, trial insertion and removal are performed in this subvolume with acceptance probability $P_{add}(v)$ and $P_{rem}(v)$, respectively. The expression for free energy of vacancy formation is then

$$F = -k_B T ln(vP_{add}(v)/P_{rem}(v)\,\Lambda^d) \tag{14}$$

in which Λ is de Broglie wavelength and d is system dimension. The vacancy concentrations can thus be calculated from free energy F, and the vacancy concentrations for pure large species are listed in the first row of Table (Ⅲ). These are very small and decrease exponentially with increasing pressure.

The possibility of substitution shifts the total equilibrium vacancy concentration (including vacancies occupied by one or more dopant) to higher values compared to the pure solid; a dopant residing in a vacancy will prevent it from being filled by a large particle[34]. The total vacancy concentration (including substituted vacancies) in the doped systems then is the concentration of unoccupied vacancies divided by the equilibrium fraction of vacancies that are unoccupied in the doped system, x_{empty} for a given dopant type and system pressure (Fig. (7)). To check the reliability of this method, we compared its predictions with the results of direct GCMC simulation incorporating large-particle insertion/removal moves for one test case (system S2 at pressure 6.0) and found an average vacancy concentration of 1.46×10^{-4}, in satisfactory agreement with the value of 1.75×10^{-4} found through the indirect method. The agreement suggests that the free energy of forming an unoccupied vacancy is the same, to a fair approximation, in the doped solids as is calculated for the pure solid.

The combined concentration of empty and substituted large-particle vacancies, shown in Table (Ⅲ), stays approximately constant in all systems with increasing pressure. Keeping in mind that the values reflect the solid-liquid coexistence condition and that increasing pressure favors configurations of high packing efficiency, this result suggests that the space-filling efficiency of the small particles occupying the vacancy sites is similar to their packing efficiency in the coexisting liquid in systems.

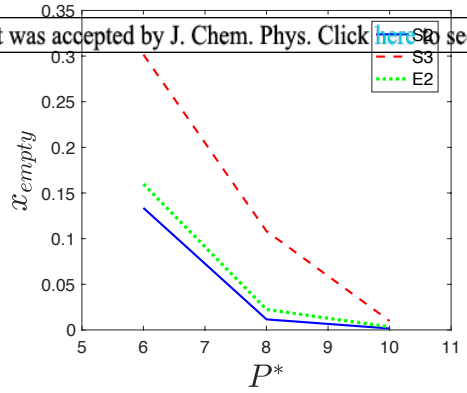

FIG. 7. Unoccupied vacancy fractions (x_{empty}) for different systems at different pressures.

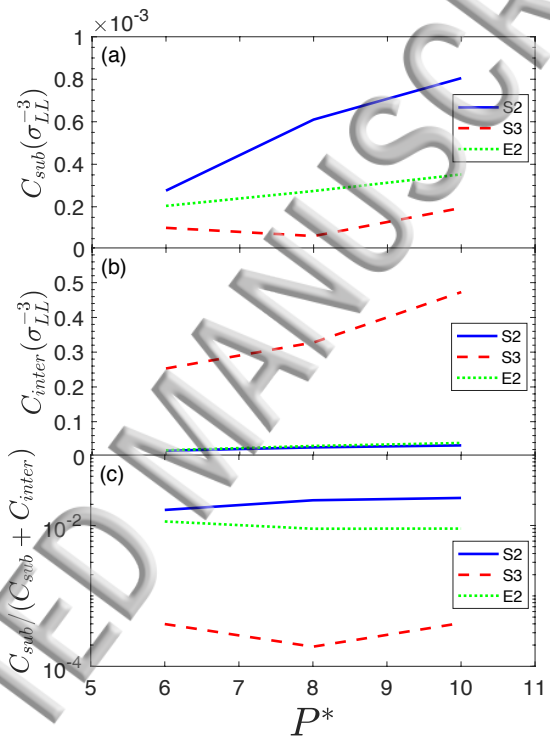

FIG. 8. (a) Concentration of substitutional particles at different pressures; (b) Concentration of interstitial particles at different pressures; (c) fraction of substitutional particles ($C_{sub}/(C_{sub}+C_{inter})$) at different pressures.

The total concentration of substitutional dopants is then the product of the total combined vacancy concentration and the average vacancy occupation, which is shown in Fig. (8) along with the total concentration of interstitial dopants. Although the probability of occupation of interstitial sites is not as large as for vacancies, the much larger number of these sites makes interstitials the majority dopant type. At most, the fraction of dopants in substitutional sites

reaches 1-2% of the interstitial dopant concentration; their levels are thus not significant for determination of the phase diagram, but could conceivably be detectable with an appropriate experiment.

Table Ⅲ. Total of unoccupied, singly, and multiply substituted large particle vacancies in solid phase at liquid-solid coexistence for different mixtures and pressures. Levels for pure systems are calculated by free energy of vacancy formation. Mixtures (S2, S3 and E2) are calculated by the vacancy concentration in pure system divided by x_{empty}, as discussed in section *3.2*.

system	$C_{vacancy}\ (\sigma_{LL}^{-3})$		
	$P^* = 6.0$	$P^* = 8.0$	$P^* = 10.0$
Pure Large	2.34×10^{-5}	2.66×10^{-6}	3.78×10^{-7}
S2	1.75×10^{-4}	2.30×10^{-4}	2.36×10^{-4}
S3	7.76×10^{-5}	2.46×10^{-5}	3.86×10^{-5}
E2	1.46×10^{-4}	1.19×10^{-4}	1.18×10^{-4}

3.3 Dynamical and structural analysis of solutes in solid solution

We took some configurations of our GCMC simulations and run only the regular translation MC moves on these configurations for system S2 at different pressures to investigate the dynamics of small-particle diffusion. Small particles in interstice have some mobility (green trajectories in Fig. (9); particles migrate between neighboring interstitial sites, similar to the behavior found in hard sphere ISS system[5]. We also observed a decrease in this mobility upon increasing the pressure, which leads to a more compact octahedron and tetrahedron hole in interstice. These trajectories were initiated with 4 small particles in a substitutional site. Small particles occupying vacancies explore the volume vacated by the large particle as well as the six neighboring octahedral holes, creating a 4-pointed star when projected on the x-y plane (red trajectories in Fig. (9). Few transitions from the vacancy zone into neighboring octahedral holes were observed, all of which returned to the vacancy during the period of observation, and (like transitions between interstitial sites) all passing through the tetrahedral sites. In some cases (like Fig. (9b)), the interstitial particle enters into the vacancy and remains there. In additional tests (not shown) we have found that interstitial particles will enter a vacancy, or leave a vacancy that is occupied by an excessive number of particles, at comparable rates to the migration between interstitial sites. So, the vacancy site appears to act as a stable trap for small particles without a particularly high barrier to enter.

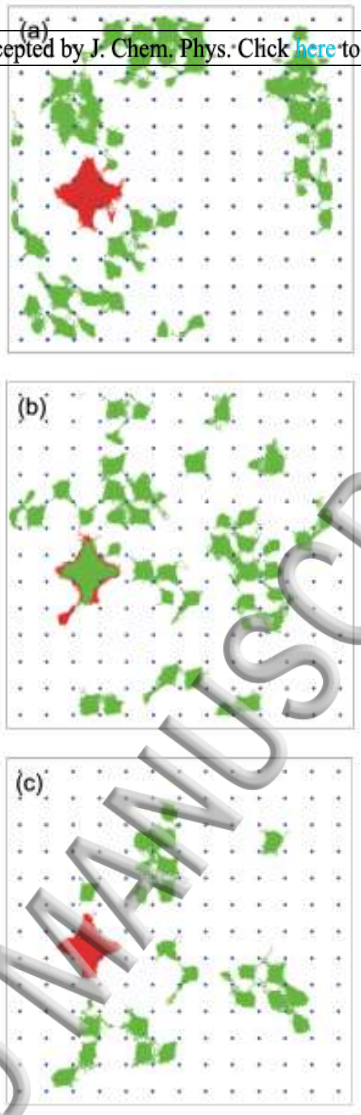

FIG. 9. The projection of a System S2 trajectory on x-y plane for small particles with initial position in vacancy (red) and interstice (green) at pressure (a) 6.0, (b) 8.0 and (c) 10.0; The blue lattice points denote the tetrahedral holes in solid.

Fig. (10) shows a close look at the probability distribution of small species in the defect site of system S2 at P^*=10.0. The probability distribution for the small species confined by the vacancy has an octahedral shape, even when there is only one small particle present (Fig. (10a)). However, when there are more particles presented (Fig. (10b)), the density distribution splits into some high probability regions and low probability regions, which indicates some structure in the arrangements of multiple small species in the defect site. The distribution of angles in the 3-fold occupied system shows most of time they formed a triangle with a maximum angle

smaller than 90° (Fig. (11)). When moving up to the case that 4 particles occupying the vacancy, a highly symmetrical tetrahedral structure would be optimal in terms of attractions between the small particles. Therefore, the orientational tetrahedral order parameter q is employed to analyze the configurations[35-36]:

$$q = 1 - \frac{3}{8}\sum_{j=1}^{3}\sum_{k=j+1}^{4}\left(cos\theta_{jk} + \frac{1}{3}\right)^2 \quad (15)$$

in which θ_{jk} is the angle formed by the lines joining the average position of four particles in consideration and the small particles j and k. For a regular tetrahedron, q will equal 1. Fig. (12) shows the major configuration is a tetrahedron as we predicted. Interestingly, there is also a second probable configuration (the second peak in Fig. (12a)), associated with a planar structure. Fig. (12b) shows the distribution of distances between the particles in the tetramer and their center of mass, whose peak is slightly above the distance (0.343 σ_{LL}) for a perfect tetrahedron with edge lengths at the potential minimum of 1.12 σ_{SS}.

A widely used order parameter Q_l developed by Steinhardt *et al.*[37] is employed to identify the cluster structure of 6-fold occupied system. Q_l is defined as:

$$Q_l = \left[\frac{4\pi}{2(l+1)}\sum_{m=-l}^{l}\left|\frac{1}{N}\sum_{j=1}^{N}Y_l^m(\theta_j,\phi_j)\right|^2\right]^{1/2} \quad (16)$$

where N is the number of lines joining the six particles in vacancy and their average position, $Y_l^m(\theta_j,\phi_j)$ is a spherical harmonic, and θ_j and ϕ_j are the angular coordinates of the jth particle with respect to some reference frame. Fig. (13) shows the Q_4 and Q_8 in our system deviates from the values in regular octahedron, although the Q_6 and Q_{10} fit the regular value quite well. We therefore cannot conclude the most probable structure in vacancy is octahedral. From visualization of the clusters in vacancy, we do see many distorted structures; only a few can be identified as the configuration close to the regular octahedron. We did not analyze the case more than 6-fold occupied system, due to the complexity of the cluster analysis when there are more particles, and the fact that it is a rare case to have an occupation larger than 6 for system S2 (Fig. (6a)).

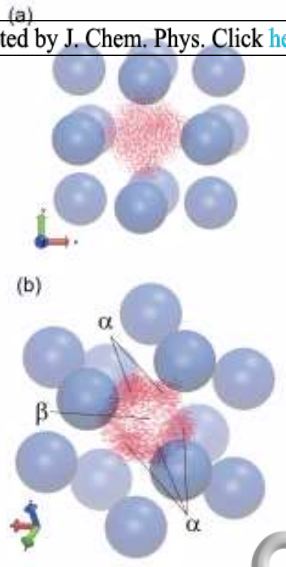

FIG. 10. Small species probability distribution plots (Red) in large species defect site for system S2 at P^*=10.0 (nearest 12 neighbors of large species are shown in transparent blue to indicate the defect site "cavity") are shown with (a) only one particle in the defect site; (b) three particles present in the defect site. α indicates the high probability region small particles presented, while β indicates the low probability region.

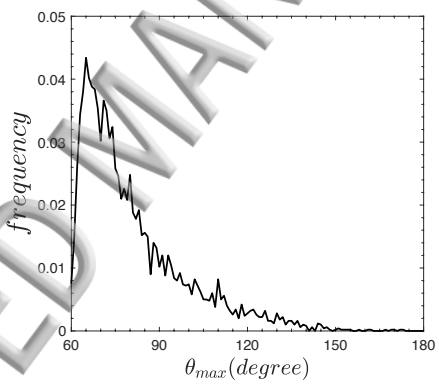

FIG. 11. The distribution of maximum angle θ_{max} in the triangle formed by the three small substitutional particles in vacancy for system S2 at P^*=10.0.

4. Conclusions

While interstitial and 1:1 substitution are well-studied modes of solution for small particles in the solid crystal formed by a larger particle type, we have quantified and characterized the degree of plural substitution in Lennard-Jones solid solutions at coexistence with fluid mixtures. The number of smaller solutes or dopants that occupy insterstitial sites was significantly greater than the number absorbed substitutionally for the three cases studied, with diameter ratios 1:2

or 1:3. Nonetheless, the phenomenon of plural substitution had a significant effect on the total number of large-particle lattice vacancies, keeping their level approximately constant as the pressure increased, in contrast to a lattice formed purely of large particles. Dynamical and structural analysis show similarities between the 1:3 LJ mixture and a similar hard-sphere interstitial solid solution, but that the Lennard-Jones particles tend toward multiple occupancy of interstitial sites as well.

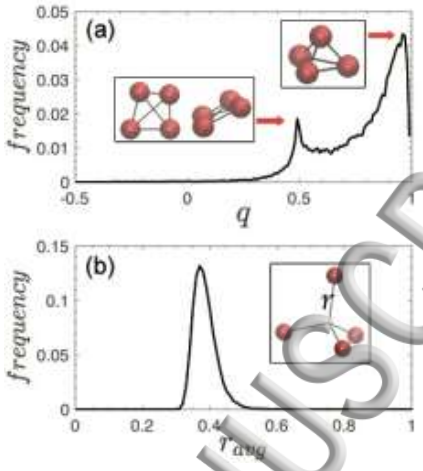

FIG. 12. Distribution of (a) orientational tetrahedral order parameter q, and (b) distance from particles to their average for four particles occupying vacancy in system S2 at P^*=10.0.

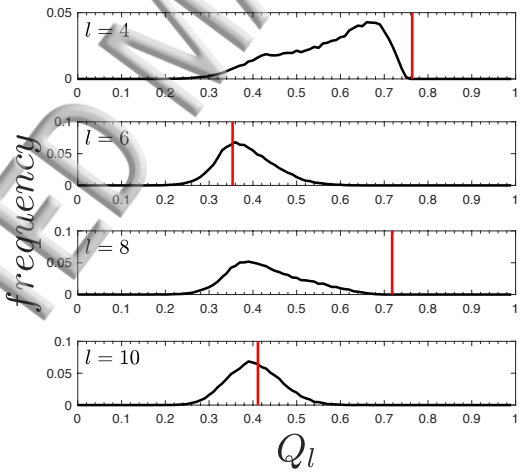

FIG. 13. Distribution of order parameter Q_l for six particles occupying vacancy in system S2 at P^*=10.0. Red vertical lines denote the Q_l for regular octahedron in corresponding l.

This manuscript was accepted by J. Chem. Phys. Click here to see the version of record.

Acknowledgments

This work used the Extreme Science and Engineering Discovery Environment (XSEDE) Comet cluster at the San Diego Supercomputer Center, which is supported by National Science Foundation grant number ACI-1548562, allocation TG-MCB110144. This work also used the resources of the Cherry L. Emerson Center for Scientific Computation.

References

1. Barroso, M.; Ferreira, A., Solid–fluid coexistence of the Lennard-Jones system from absolute free energy calculations. *J. of Chem. Phys.* **2002,** *116* (16), 7145-7150.
2. Trizac, B. E.; Madden, M. E.; PA, Stability of the AB crystal for asymmetric binary hard sphere mixtures. *Molecular Physics* **1997,** *90* (4), 675-678.
3. Hunt, N.; Jardine, R.; Bartlett, P., Superlattice formation in mixtures of hard-sphere colloids. *Physical Review E* **2000,** *62* (1), 900.
4. Vermolen, E.; Kuijk, A.; Filion, L.; Hermes, M.; Thijssen, J.; Dijkstra, M.; Van Blaaderen, A., Fabrication of large binary colloidal crystals with a NaCl structure. *Proceedings of the National Academy of Sciences* **2009,** *106* (38), 16063-16067.
5. Filion, L.; Hermes, M.; Ni, R.; Vermolen, E.; Kuijk, A.; Christova, C.; Stiefelhagen, J.; Vissers, T.; van Blaaderen, A.; Dijkstra, M., Self-assembly of a colloidal interstitial solid with tunable sublattice doping. *Physical Review Letters* **2011,** *107* (16), 168302.
6. Verhoeven, J. D., *Steel metallurgy for the non-metallurgist*. ASM International: 2007.
7. Schofield, A.; Pusey, P.; Radcliffe, P., Stability of the binary colloidal crystals A B 2 and A B 13. *Physical Review E* **2005,** *72* (3), 031407.
8. Paxton, A.; Elsässer, C., Analysis of a carbon dimer bound to a vacancy in iron using density functional theory and a tight binding model. *Physical Review B* **2013,** *87* (22), 224110.
9. Wang, Z.; Liu, C.; Dou, P., Thermodynamics of vacancies and clusters in high-entropy alloys. *Physical Review Materials* **2017,** *1* (4), 043601.
10. Fernández, J. R.; Harrowell, P., Crystal phases of a glass-forming Lennard-Jones mixture. *Physical Review E* **2003,** *67* (1), 011403.
11. Middleton, T. F.; Hernández-Rojas, J.; Mortenson, P. N.; Wales, D. J., Crystals of binary Lennard-Jones solids. *Physical Review B* **2001,** *64* (18), 184201.
12. Gusev, A. A.; Lurie, S. A., Strain - Gradient Elasticity for Bridging Continuum and Atomistic Estimates of Stiffness of Binary Lennard - Jones Crystals. *Advanced Engineering Materials* **2010,** *12* (6), 529-533.
13. Phillips, C. L.; Crozier, P. S., An energy-conserving two-temperature model of radiation damage in single-component and binary Lennard-Jones crystals. *Journal of Chemical Physics* **2009,** *131* (7), 074701.
14. Jungblut, S.; Dellago, C., Crystallization of a binary Lennard-Jones mixture. *Journal of Chemical Physics* **2011,** *134* (10), 104501.
15. Fernández, J. R.; Harrowell, P., Ordered binary crystal phases of Lennard-Jones mixtures. *Journal of Chemical Physics* **2004,** *120* (19), 9222-9232.
16. Vlot, M. J.; Huitema, H. E.; de Vooys, A.; van der Eerden, J. P., Crystal structures of symmetric Lennard-Jones mixtures. *Journal of Chemical Physics* **1997,** *107* (11), 4345-4349.

17. Cook, S. J.; Clancy, P., Impurity segregation in Lennard-Jones A/AB heterostructures. I. The effect of interstitial impurities. *Journal of Chemical Physics* **1993,** *99* (3), 2175-2191.
18. Cook, S. J.; Clancy, P., Impurity segregation in Lennard-Jones A/AB heterostructures. II. The effect of impurity size. *Journal of Chemical Physics* **1993,** *99* (3), 2192-2201.
19. Sweatman, M.; Quirke, N., Simulating fluid–solid equilibrium with the Gibbs ensemble. *Molecular Simulation* **2004,** *30* (1), 23-28.
20. Shetty, R.; Escobedo, F. A., On the application of virtual Gibbs ensembles to the direct simulation of fluid–fluid and solid–fluid phase coexistence. *Journal of Chemical Physics* **2002,** *116* (18), 7957-7966.
21. Errington, J. R., Solid–liquid phase coexistence of the Lennard-Jones system through phase-switch Monte Carlo simulation. *Journal of Chemical Physics* **2004**, *120* (7), 3130-3141.
22. Cottin, X.; Monson, P., Solid–fluid phase equilibrium for single component and binary Lennard-Jones systems: A cell theory approach. *Journal of Chemical Physics* **1996,** *105* (22), 10022-10029.
23. Radu, M.; Kremer, K., Enhanced Crystal Growth in Binary Lennard-Jones Mixtures. *Physical Review Letters* **2017,** *118* (5), 055702.
24. Kofke, D. A., Direct evaluation of phase coexistence by molecular simulation via integration along the saturation line. *Journal of Chemical Physics* **1993,** *98* (5), 4149-4162.
25. Kofke, D. A., Gibbs-Duhem integration: a new method for direct evaluation of phase coexistence by molecular simulation. *Molecular Physics* **1993,** *78* (6), 1331-1336.
26. Hitchcock, M. R.; Hall, C. K., Solid–liquid phase equilibrium for binary Lennard-Jones mixtures. *The Journal of chemical physics* **1999,** *110* (23), 11433-11444.
27. Lamm, M. H.; Hall, C. K., Equilibria between solid, liquid, and vapor phases in binary Lennard–Jones mixtures. *Fluid Phase Equilibria* **2002,** *194*, 197-206.
28. Sherwood, A.; Prausnitz, J., Intermolecular potential functions and the second and third virial coefficients. *Journal of Chemical Physics* **1964,** *41* (2), 429-437.
29. Bennett, C.; Alder, B., Studies in Molecular Dynamics. IX. Vacancies in Hard Sphere Crystals. *Journal of Chemical Physics* **1971,** *54* (11), 4796-4808.
30. Bowles, R. K.; Speedy, R. J., Cavities in the hard sphere crystal and fluid. *Molecular Physics* **1994,** *83* (1), 113-125.
31. Humphrey, W.; Dalke, A.; Schulten, K., VMD: visual molecular dynamics. *Journal of Molecular Graphics* **1996,** *14* (1), 33-38.
32. Kindt, J. T., Grand canonical Monte Carlo using solvent repacking: Application to phase behavior of hard disk mixtures. *Journal of Chemical Physics* **2015,** *143* (12), 124109.
33. Guo, Z.; Kindt, J. T., Gibbs ensemble Monte Carlo with solvent repacking: phase coexistence of size–asymmetrical binary Lennard-Jones mixtures. *Molecular Simulation* **2017**, 1-9.
34. Schuler, T.; Barouh, C.; Nastar, M.; Fu, C.-C., Equilibrium vacancy concentration driven by undetectable impurities. *Physical Review Letters* **2015,** *115* (1), 015501.
35. Chau, P.-L.; Hardwick, A., A new order parameter for tetrahedral configurations. *Molecular Physics* **1998,** *93* (3), 511-518.
36. Duboué-Dijon, E.; Laage, D., Characterization of the local structure in liquid water by various order parameters. *Journal of Physical Chemistry B* **2015,** *119* (26), 8406-8418.
37. Steinhardt, P. J.; Nelson, D. R.; Ronchetti, M., Bond-orientational order in liquids and glasses. *Physical Review B* **1983,** *28* (2), 784.

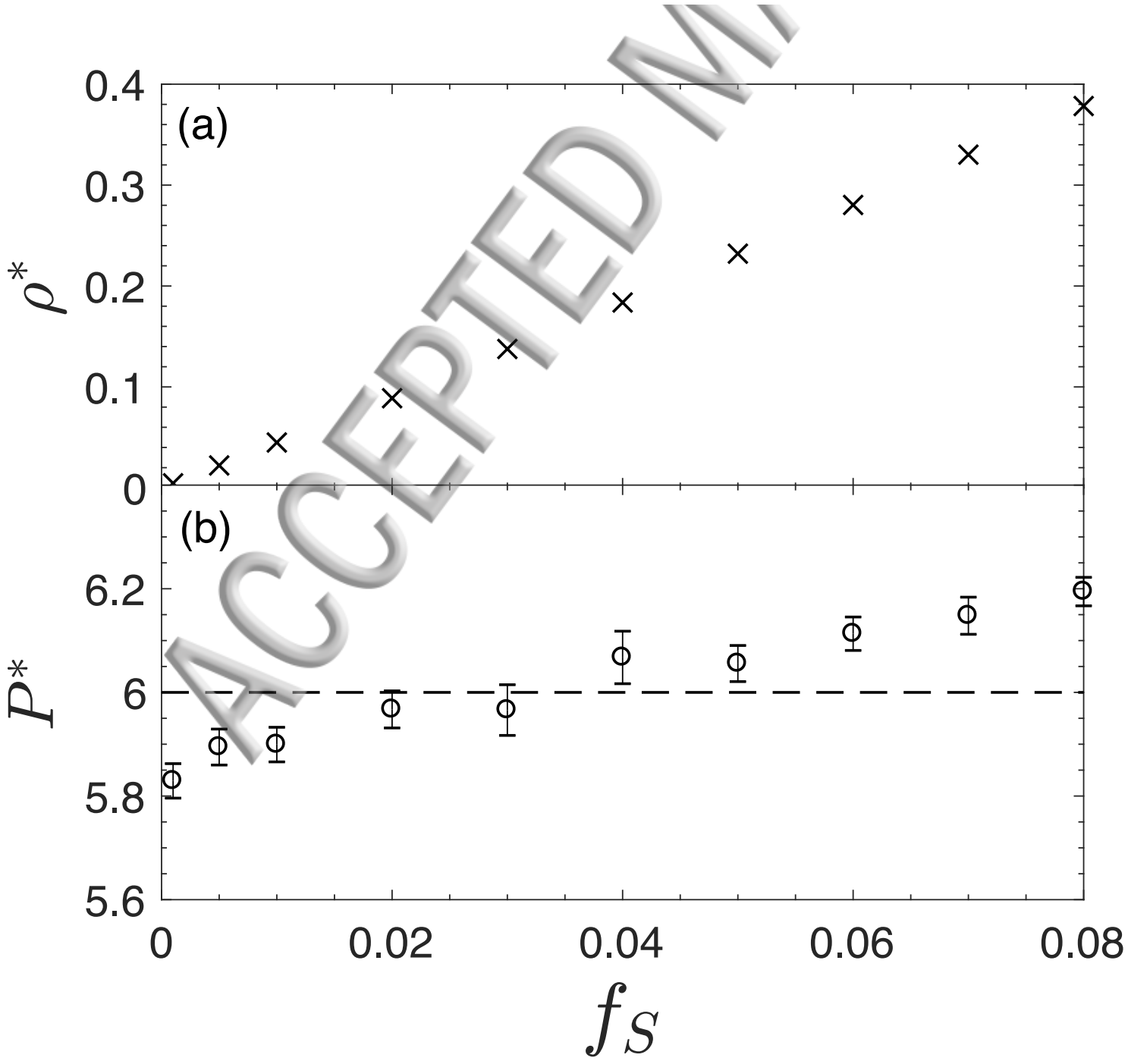

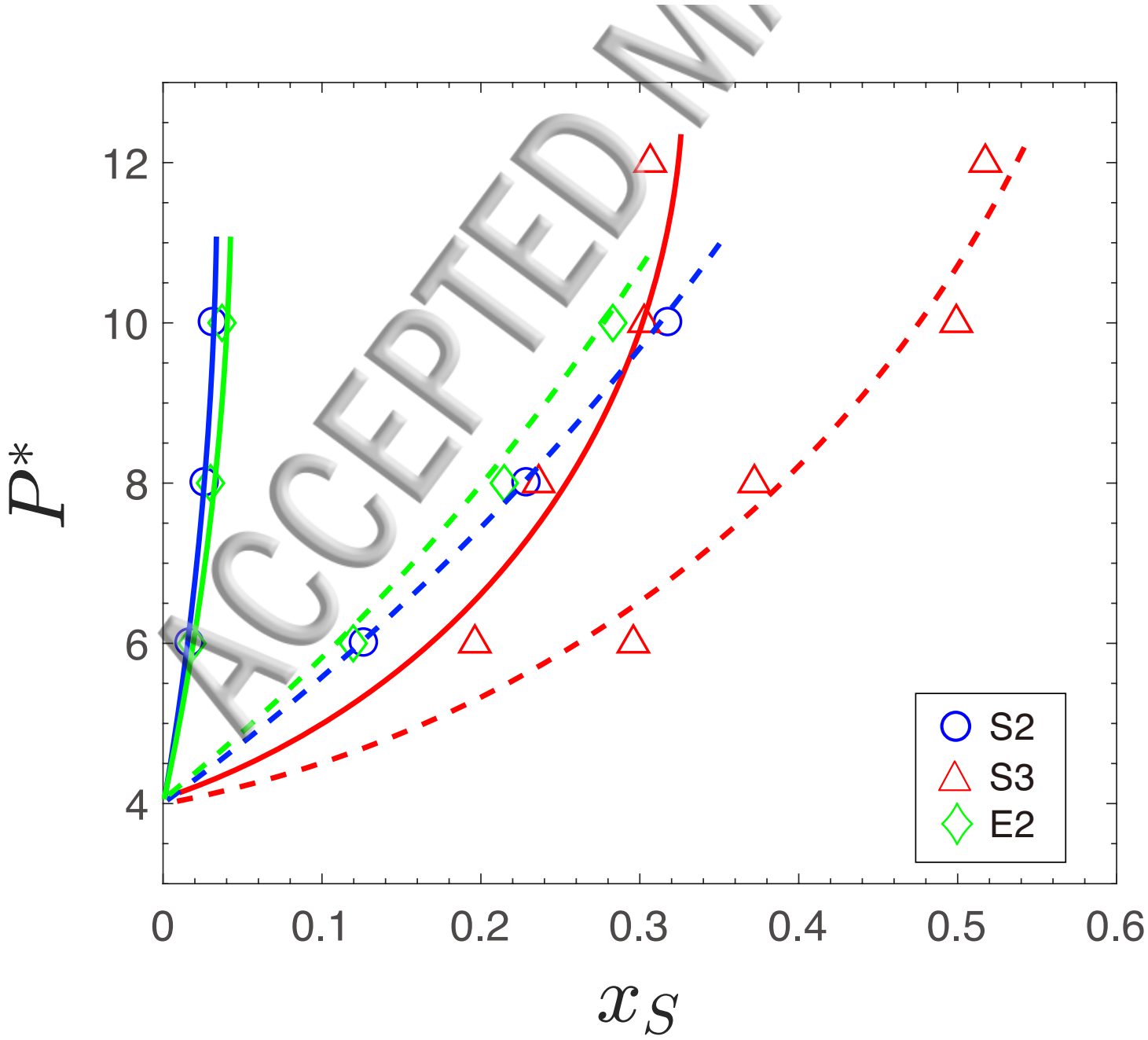

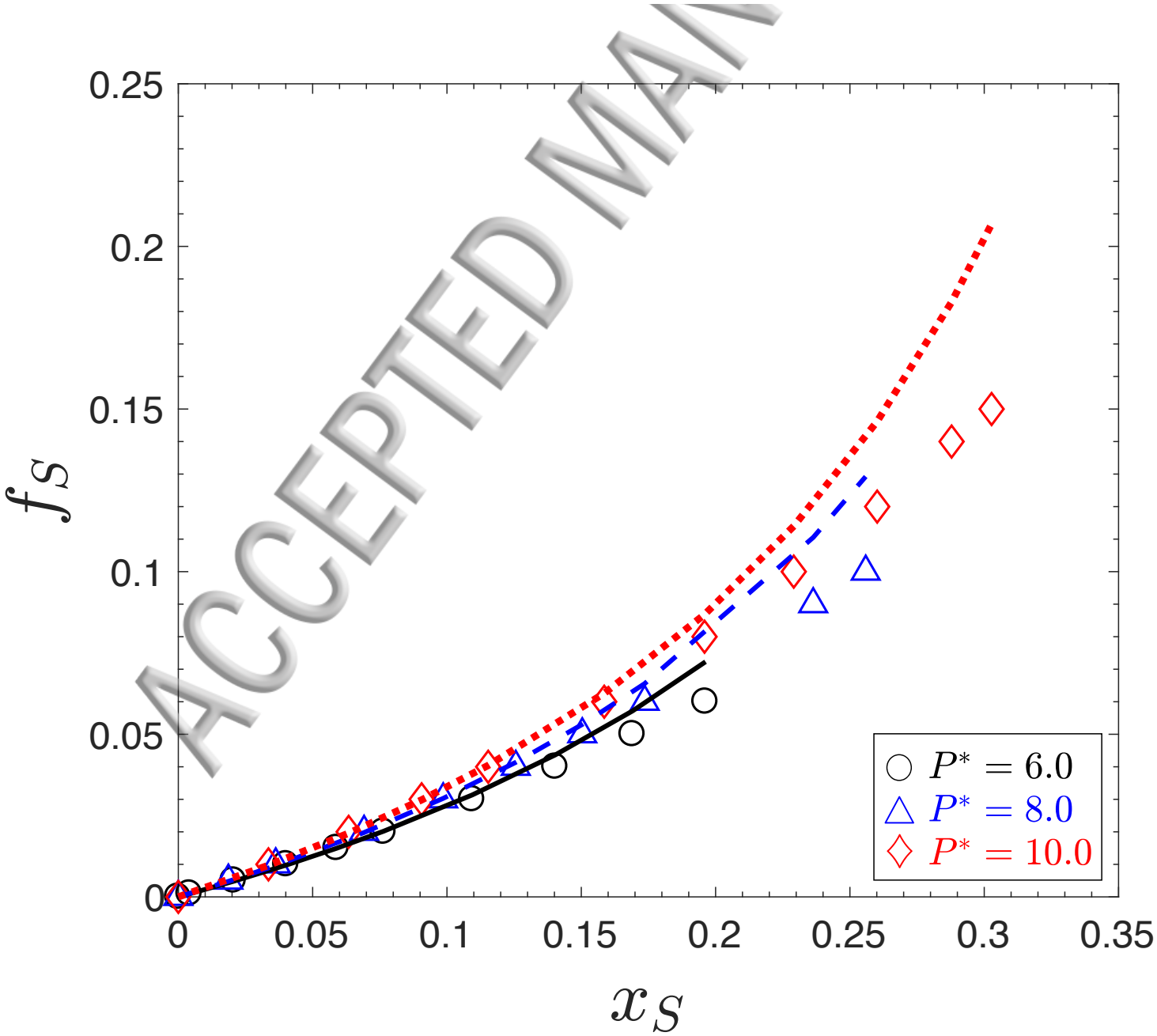

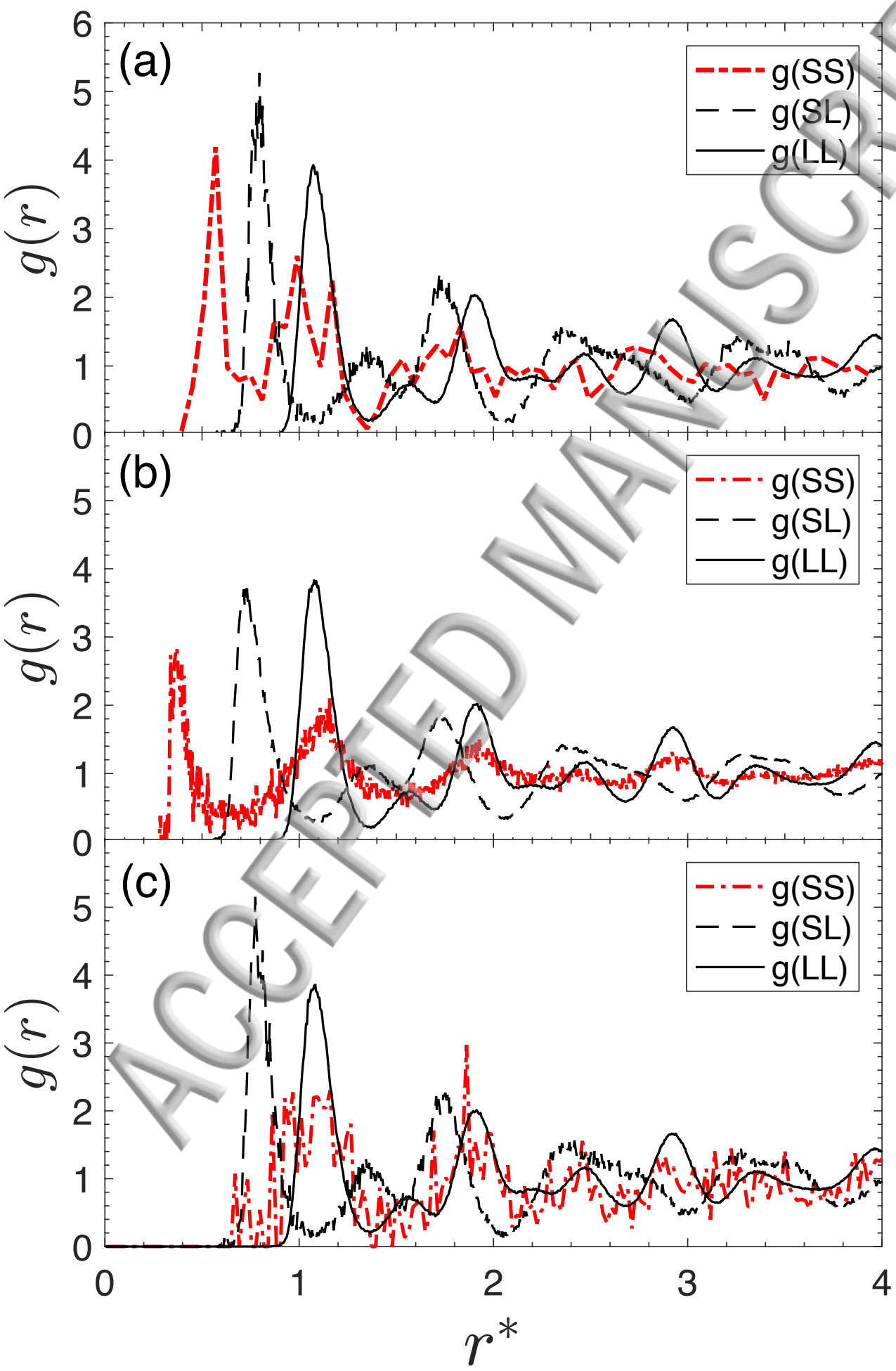

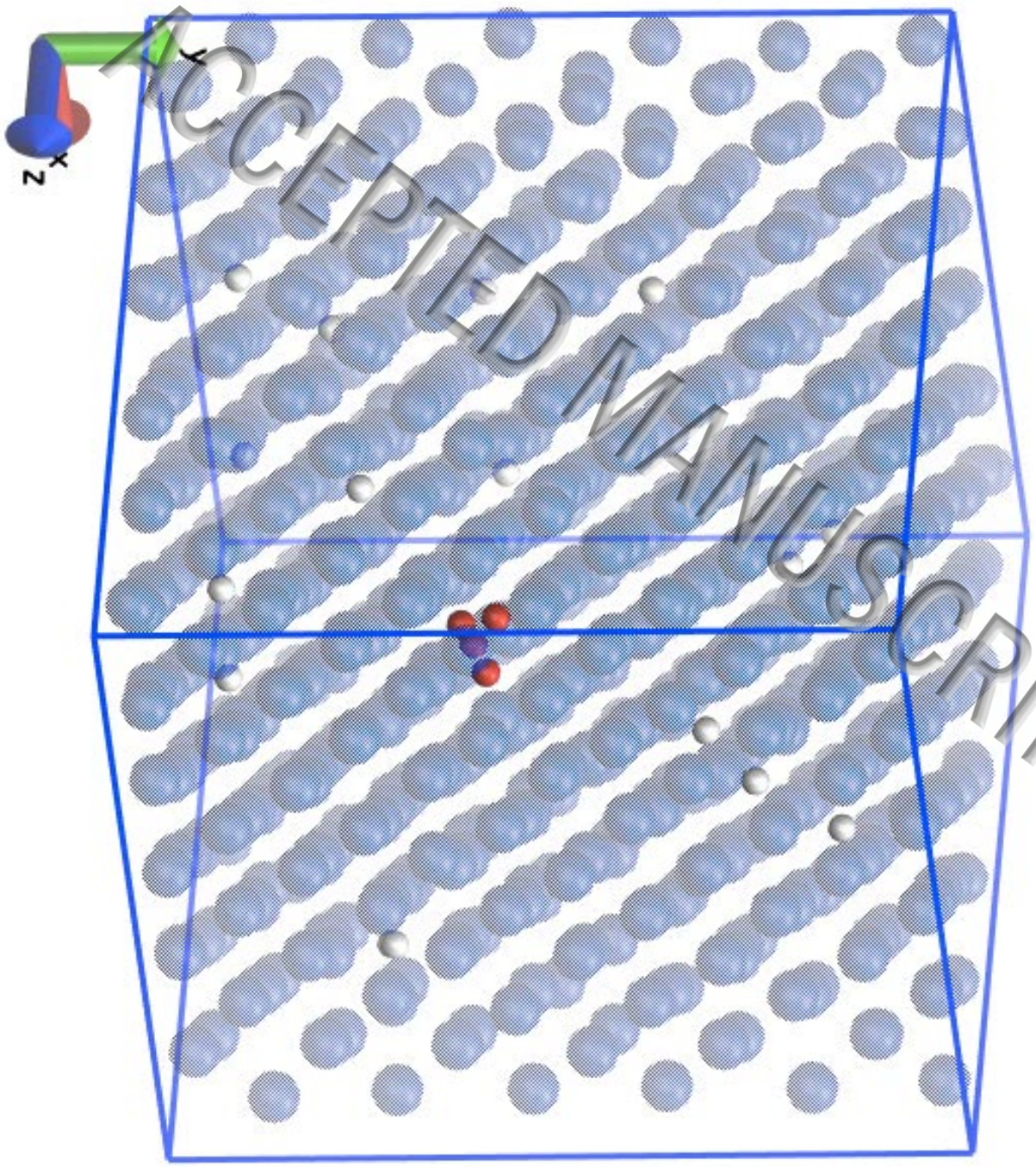

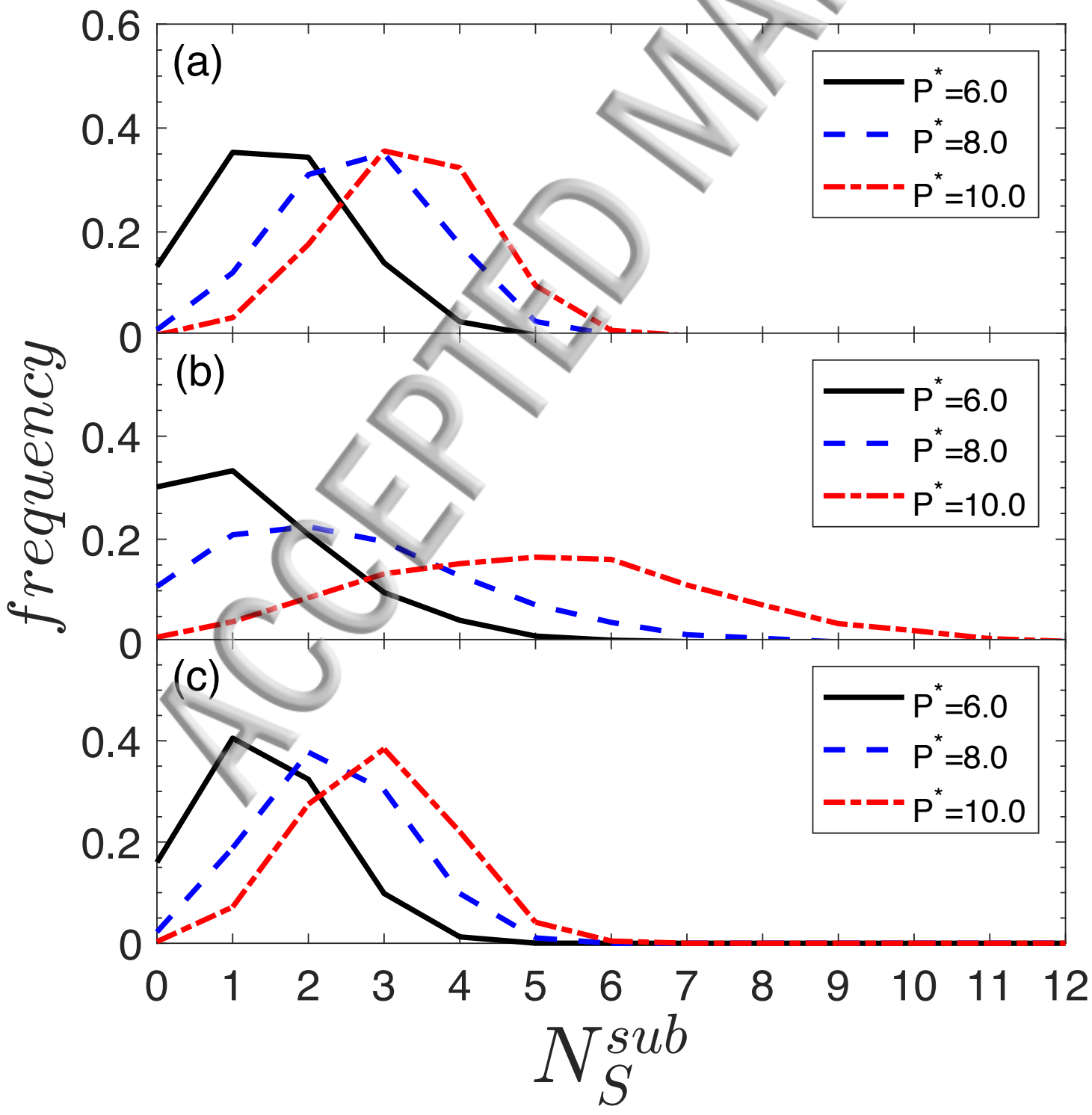

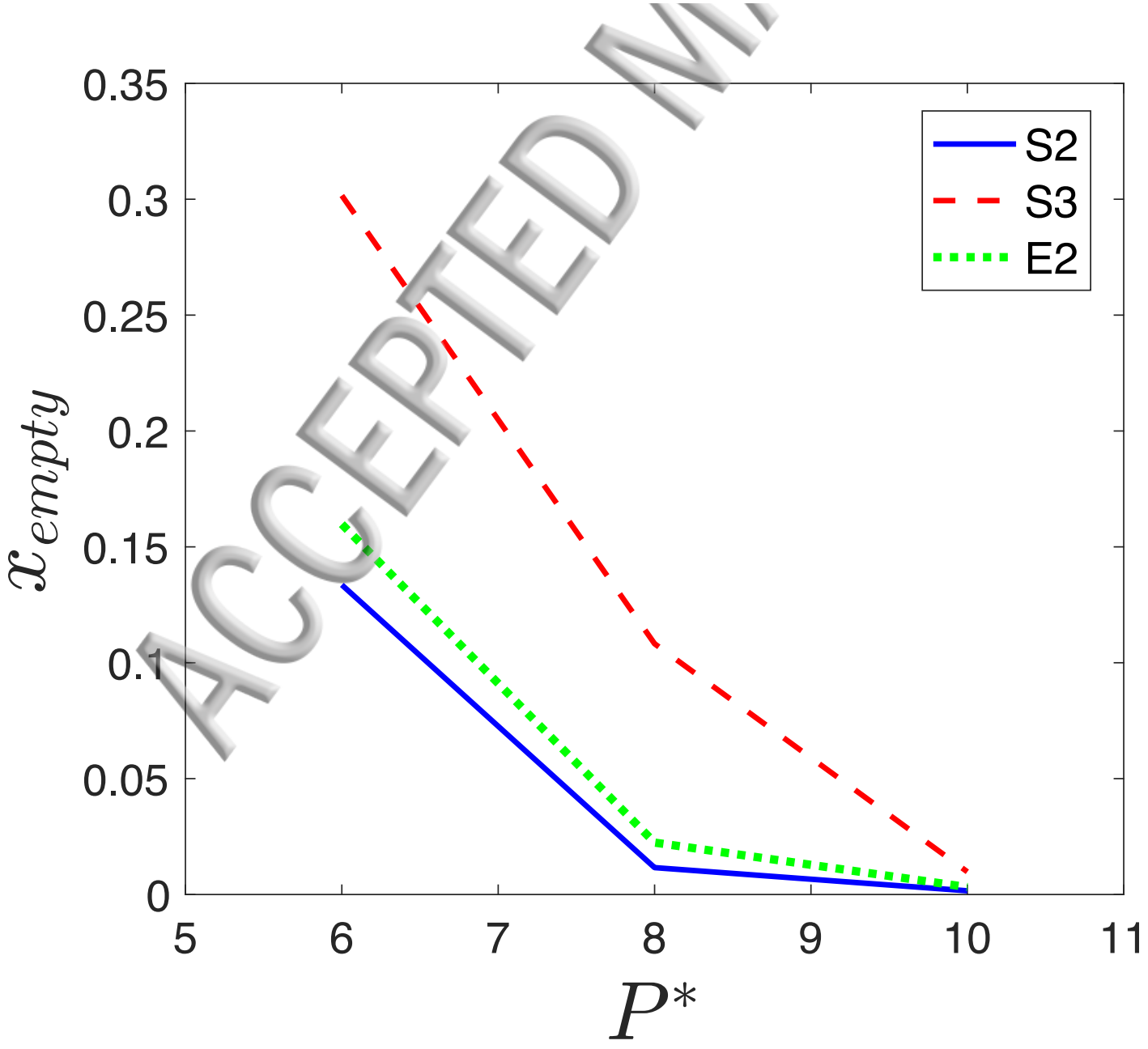

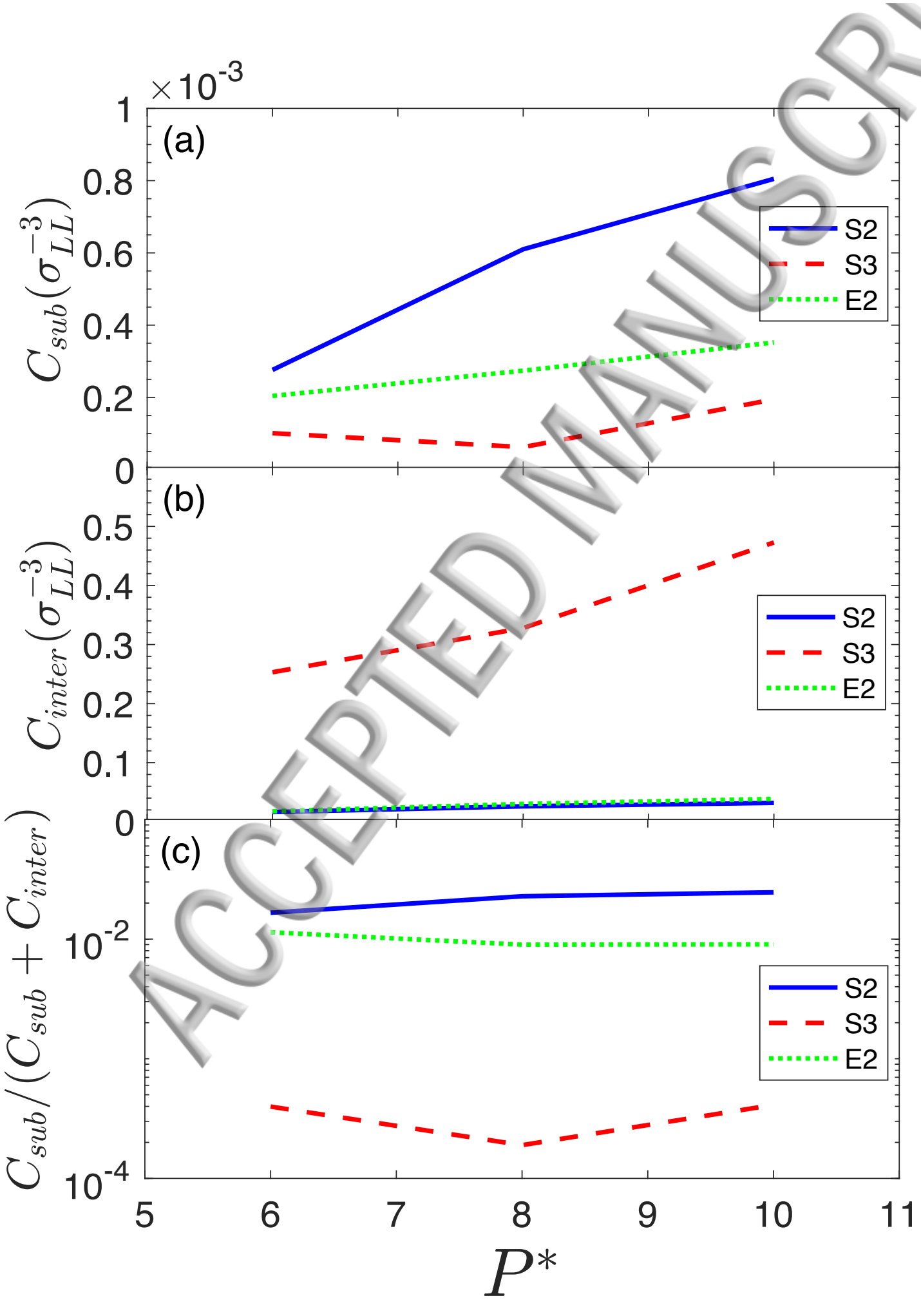

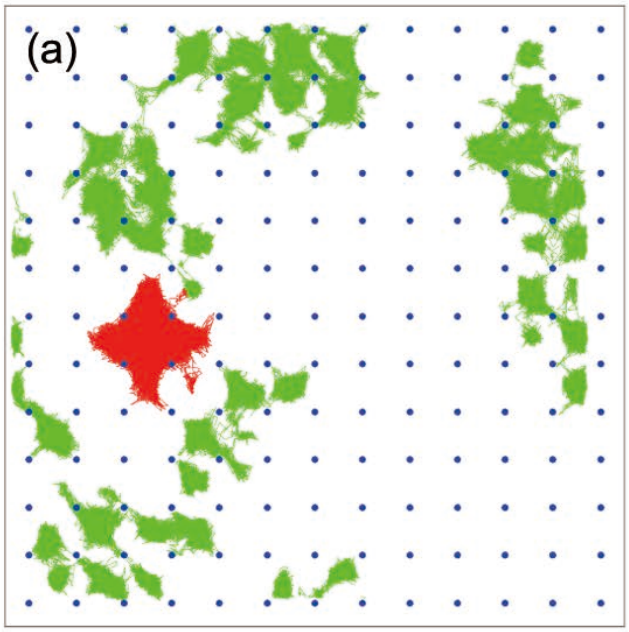

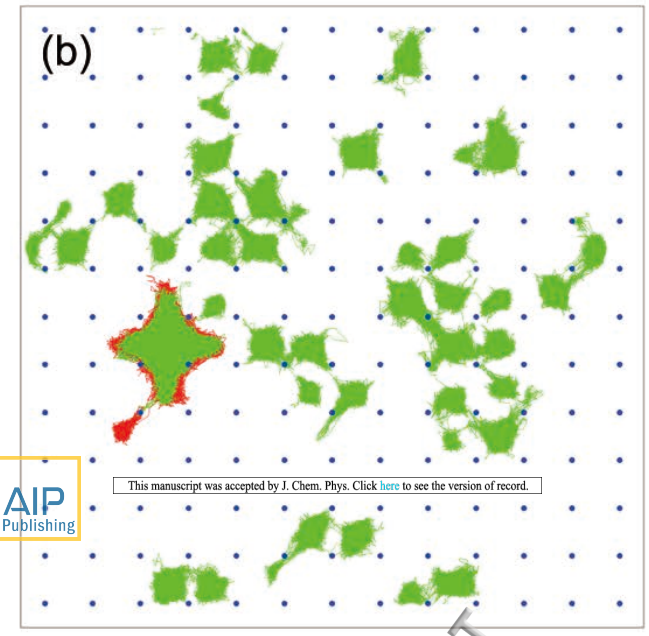

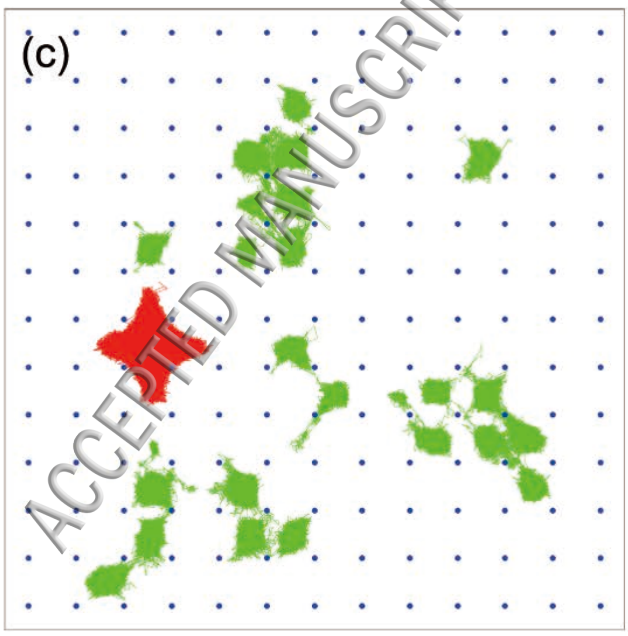

(a)

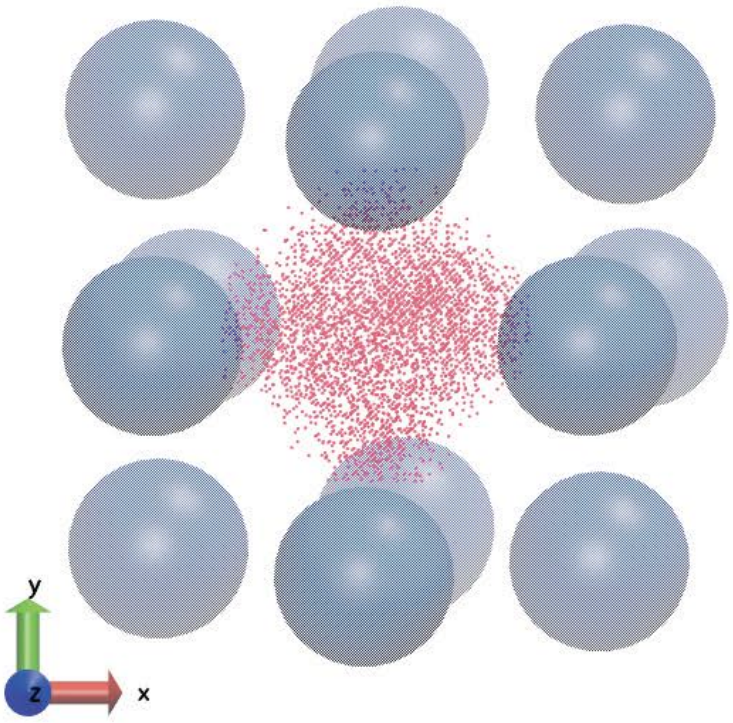

This manuscript was accepted by J. Chem. Phys. Click here to see the version of record.

(b)